Novel shape indices for vector landscape pattern analysis

The formation of an anisotropic landscape is influenced by natural and/or human processes, which can then be inferred on the basis of geometric indices. In this study, two minimal bounding rectangles in consideration of the principles of mechanics (i.e. minimal width bounding (MWB) box and moment bounding (MB) box) were introduced. Based on these boxes, four novel shape indices, namely MBLW (the length-to-width ratio of MB box), PAMBA (area ratio between patch and MB box), PPMBP (perimeter ratio between patch and MB box) and ODI (orientation difference index between MB and MWB boxes), were introduced to capture multiple aspects of landscape features including patch elongation, patch compactness, patch roughness and patch symmetry. Landscape pattern was, thus, quantified by considering both patch directionality and patch shape simultaneously, which is especially suitable for anisotropic landscape analysis. The effectiveness of the new indices were tested with real landscape data consisting of three kinds of saline soil patches (i.e. the elongated shaped slightly saline soil class, the circular or half-moon shaped moderately saline soil, and the large and complex severely saline soil patches). The resulting classification was found to be more accurate and robust than that based on traditional shape complexity indices.

Keywords: landscape metrics; anisotropy; moment box; patch elongation; patch symmetry

1 Introduction

Landscape patterns may be defined as sets of landscape observations with spatial structure and which are, thus, significantly different from the realization of a random process. These patterns contain information on the mechanisms or processes from which they emerge (Grimm *et al.* 2005, Schröder and Seppelt 2006). Quantifying landscape patterns is, thus, considered to be a prerequisite for the study of pattern-process relationships (Turner 1990, Uuemaa *et al.* 2013), a fundamental pursuit of landscape ecology (Turner 2005, Helfenstein *et al.* 2014). Landscape pattern analysis based on the patch-matrix model (i.e. landscape pattern indices (LPIs)) or the gradient model (McGarigal *et al.* 2009) has, therefore, received increasing attention in both ecological research and the environmental management communities (Cissel *et al.* 1999, Fu and Chen 2000, Turner 2005).

In line with human interpretation of real landscapes (Lausch et al. 2015), landscape pattern indices (LPIs) offer an effective way to capture landscape structure, with either landscape-, class-, or patch-focus (McGarigal and McComb 1995, Kupfer 2012). This has increased our understanding of the relationships between spatial patterns and ecological processes on a range of scales (Wu 2013). As a popular quantitative analysis tool (Schröder and Seppelt 2006), LPIs have been applied increasingly to a variety of issues in landscape ecology (Uuemaa *et al.* 2013, Lausch *et al.* 2015), for example, assessment of landscape patterns or changes in land cover/use (Seto and Fragkias 2005; Reddy *et al.* 2013; Van Den Hoek *et al.* 2015), inference of landscape functions (Bolliger *et al.* 2007; Li *et al.* 2015), and quantification of ecosystem services (Syrbe and Walz 2012). The rapid advancement of remote sensing and geographic information systems (GIS) has also promoted the development and utilization of LPIs. During the past 30 years, numerous LPIs have been developed to quantify different spatial and compositional aspects of landscape structure (Lausch *et al.* 2015), and they are derived variously from fractal geometry (Krummel *et al.* 1987, Li 2000), information theory (O'Neill *et al.* 1988), percolation theory (Gardner and O'Neill 1991), statistical measures of dispersion (Gertsev 2004), mechanics (Zhang *et al.* 2006) and mathematical morphology (Vogt *et al.* 2007). Most of these indices can be computed readily by accessible software (e.g., 'r.le' and 'FRAGSTATS') to facilitate their implementation (Baker and Cai 1992, McGarigal and McComb 1995, Remmel and Fortin 2013).

In the face of complicated and diversified geographic landscapes, LPIs exhibit certain deficiencies and limitations. In particular, some LPIs provide ambiguous information about spatial patterns. For example, one landscape index may have the same numerical value for drastically different landscapes (Gustafson and Parker 1992, Tischendorf 2001, Corry and Nassauer 2005), while several visually distinct spatial patterns may exhibit similar LPI values (Remmel and Csillag 2003, Turner 2005). One important ambiguity is that most shape complexity indices (including many fractal methods) are derived based on a form of perimeter-area relationship (Forman and Godron 1986, Riitters *et al.* 1995, Gustafson 1998) and, for example, ignore the directional differences between patches. Current landscape metrics actually belong to indices of scalar quantity, that is, with loss of a patch's vector dimension (Zhang *et al.* 2006), which may result in uncertainties in shape identification. Considering a "curved" patch and an elongated linear patch, for example, both may have equal area and perimeter (i.e. their shape complexity or fractal indices might be exactly the same), but are nevertheless shaped distinctively.

Spatial anisotropy, the variation in spatial autocorrelation with orientation or direction, is often found in ecological variables because spatial patterns are sometimes produced by directional natural phenomena such as wind, fire, floods and tectonics (e.g. Legendre and Fortin 1989; Rossi *et al.* 1992; Gustafson 1998; Wu et al. 2000; Zhang *et al.* 2006). Meanwhile, human activities may also introduce a directional influence on landscapes. For example, tillage often leads to an anisotropic distribution of properties of the land surface (Vidal Vázquez *et al.* 2005). Moreover, spatial anisotropy is often associated with important ecological functions. For instance, landscape anisotropy has a direct effect on wetland flooding dynamics (Kaplan *et al.* 2012, Yuan *et al.* 2015) and the combined effects of soil anisotropy and topographic slope significantly affect the soil moisture regime by controlling the movement of water across and through the landscape (Zaslavsky and Rogowski 1969). Spatial anisotropy, therefore, plays a crucial role in real landscape analysis, which allows us to better understand the corresponding landscape pattern-process relations and landscape functions. For example, based on variogram and angular wavelet analysis, the directional process underpinning Bronze Age surface pottery in the northern Murghab Delta was identified: specifically, the impact of the complex system of watercourses in the delta on both settlement and post-depositional processes (Markofsky and Bevan 2012). However, the variogram is a geostatistical tool and is, thus, not appropriate for quantifying anisotropy in terms of the geometry of *objects* and, thus, related *patch*-based models. Consequently, it is necessary to develop landscape indices by considering the shape properties of a patch and its directional distribution simultaneously, that is, vector landscape pattern analysis (Zhang *et al.* 2006).

Zhang *et al.* (2006) first utilized the moment orientation (MO) index to represent patch orientation, based on planar characteristics defined by the principles of mechanics such as the moment of inertia, product of inertia and major/minor principal axes. The index was used to identify Qianan lakes (located in the central part of this paper's study area), whose orientations were heavily affected by the prevailing wind. However, shape complexity did not include the patch's anisotropy. Therefore, the minimum width bounding (MWB) box and the moment bounding (MB) box on the basis of the MO, were introduced here simultaneously. Based on these two boxes, novel landscape indices for vector landscape pattern analysis were proposed:

(1) patch length-to-width ratio,
(2) area ratio between patch and MB box,
(3) perimeter ratio between patch and MB box,

(4) orientation difference index between MWB box and MB box.

The effectiveness of the proposed indices was tested in this paper by identifying different types of saline soils in the western part of the Songnen plain, China. These different types of saline soil are located in different parts of a large paleolake that have specific geographic conditions. Accurate discrimination of these saline soils would be potentially useful for landscape management. However, while they vary from each other in salinity level, they have similar remote sensing spectra. For this reason, classification of the soil types based on traditional remote sensing classification approaches that depend primarily on reflectance spectra is of limited accuracy. Consequently, we investigate the additional class separability that can be attained by application of the novel shape descriptors above to the landscape patches. While it is clear that anisotropy plays a key role in determining landscape processes, or indicating the nature of the underlying landscape processes, this paper seeks to test the specific hypothesis that anisotropy and related shape indices can increase the accuracy of classification of objects in the object-based image analysis (OBIA) sense. Since these indices can be generated automatically, if they are ignored in classification analysis, this simply means that the accuracy of classification may be less than it would be if they were included.

2 Novel shape indices

2.1 Minimum Width Bounding (MWB) box

The minimum width bounding (MWB) box, in computational geometry, generally refers to the smallest enclosing rectangle with the least width over two-dimensional space (Chaudhuri and Samal 2007). The properties of a MWB box are translation, rotation and reflection invariance in terms of its enclosing polygon, thus, indicating the corresponding orientation of the original polygon.

The construction of the MWB box in this research is largely dependent on the spatial distribution of the vertices along the boundary of the polygon. A least square linear regression is first applied to fit a line, followed by an axis transformation to the local coordinate system. The bounding box can then be built up based on the maximum projections of each vertex on the new axis. Since the vertex density and spatial distribution often influence the size of the bounding box, which is not the desired MWB box in most cases, the MWB box is searched numerically by the so-called “rotation calliper” method given a user-defined threshold (Toussaint 1983). Detailed steps for building the MWB box are given below:

Step 1: Least square approximation to fit a line (Stigler 1981)

The linear function minimizing the squared errors can be calculated as:

$$f(x) = b_0 + b_1 x \tag{1}$$

The two regression parameters (b_0, b_1) can be estimated as (Equation 2 to 3):

$$b_1 = \frac{\sum xy - n\bar{x}\bar{y}}{\sum x^2 - n(\bar{x})^2} \tag{2}$$

$$b_0 = \bar{y} - b_1 \bar{x} \tag{3}$$

Where

$$\bar{x} = \frac{1}{n}\sum_{i=1}^{n} x_i \tag{4}$$

$$\bar{y} = \frac{1}{n}\sum_{i=1}^{n} y_i \tag{5}$$

$$\sum xy = \sum_{i=1}^{n} x_i y_i \tag{6}$$

$$\sum x^2 = \sum_{i=1}^{n} (x_i)^2 \quad (7)$$

In Equations 1 to 7, the parameter b_1 is the slope of the fitted line, and the variable n is the number of vertices of each polygon.

Step 2: Coordinate transformation based on the estimated slope

Coordinate transformation based on the fitted line is given by

$$\theta = \arctan(b_1) \quad (8)$$

Therefore, $\sin\theta$ and $\cos\theta$ for coordinate transformation can be calculated via Equation 8. Given a vertex (x, y) in a global coordinate system with origin (x_0, y_0), the new coordinate (x', y') can be extracted by coordinate translation and rotation (Equation 9).

$$\begin{pmatrix} x' \\ y' \end{pmatrix} = \begin{pmatrix} \cos\theta & \sin\theta \\ -\sin\theta & \cos\theta \end{pmatrix} \begin{pmatrix} x - x_0 \\ y - y_0 \end{pmatrix} + \begin{pmatrix} b_0 \cos\theta \\ b_0 \sin\theta \end{pmatrix} \quad (9)$$

By translating and rotating the axes, the *x*-axis in the new coordinate system is defined along the fitted line. A point on the *x*-axis is selected randomly as the origin of the new coordinate system, and the *y*-axis is defined perpendicular to the new *x*-axis.

Step 3: Finding the maximum and minimum coordinates of the vertices

Under the new coordinate system, the maximum and minimum *y*-coordinates of the vertices, Y_{min} and Y_{max}, as well as those of the *x*-coordinates, X_{min} and X_{max}, can be determined, which then can be used as the initial minimum bounding box.

Step 4: Rotating calliper to search the MWB box numerically

The main axis fitted by least squares approximation is influenced largely by vertex density and distribution. Therefore, it is necessary to turn the initial minimum bounding box in discrete angular steps (Lewis *et al.* 1997) to locate the rectangle bounding box with minimum width, (i.e. the MWB box). The initial angle for each rotation is set as θ, iteratively increasing or decreasing by a small angle (predefined as δ) to find the bounding box with minimum width or approximate to the minimum, which is the minimum width bounding (MWB) box with orientation θ_{MWB}.

2.2 Moment Bounding (MB) box

The MB box is the minimal bounding rectangle built upon the moment orientation (MO) (the orientation of the major axis), which is derived from planar characteristics defined by mechanics (Zhang *et al.* 2006). The MO is reviewed briefly as follows:

Suppose that (x, y) is a point within a planar polygon (S) (Figure 1), whose centroid is $C(\bar{x}, \bar{y})$, and the moment of inertia about the x-axis (I_{xx}) and about the y-axis (I_{yy}), as well as the product of inertia (I_{xy}), respectively, are expressed by Equations 10, 11 and 12.

$$I_{xx} = \int y^2 dA \tag{10}$$

$$I_{xy} = \int x^2 dA \tag{11}$$

$$I_{xy} = \int xydA \tag{12}$$

Figure 1 is here.

Note, $dA (= dx \cdot dy)$ refers to is the differential area of point (x, y) (Timoshenko and Gere 1972).

There are two orthogonal axes (called major and minor axes) passing through the centroid, which have the maximum and minimum moment of inertia about the minor and major axes, respectively. The moment orientation (MO) θ_{MB} (i.e. the orientation of the major axis) is calculated by Equations 13 and 14 (Timoshenko and Gere 1972). The moment bounding (MB) box that minimally encloses the polygon is then constructed by taking θ_{MB} as the orientation of the long side of the MB box. Equations 10-14, in discrete form suitable for patch computation, are deduced by applying Green's theorem which relates the value of a line integral to that of a double integral (see Zhang *et al.* (2006) for details).

$$\tan 2\theta_{MB} = \frac{2I_{xy}}{I_{yy} - I_{xx}} \quad (13)$$

$$\theta_{MB} = \frac{1}{2}\tan^{-1}\left(\frac{2I_{xy}}{I_{yy} - I_{xx}}\right) \quad (14)$$

2.3 Novel shape indices

Figure 2 shows the relations among a polygon (in black), its MWB box (in blue) and MB box (in red). Here, *C* is the centroid of the polygon. *PQ* is the minor axis of the MB box, about which the moment of inertia of the polygon is the maximum; *MN* is the major axis of the MB box, about which the moment of inertia of the polygon is the minimum. *AB* (*EF*), along the truck line of the long (short) side of the MWB box, is the major (minor) axis of the MWB box; *E'F'* is the line passing through *C* and parallel to the MWB box's long side. ∠*MCE'* is the angle between the two boxes, that is, the orientation difference between the two major axes (*MN* and *EF*) of the boxes. In the figure, *MN* is deflected clockwise relative to *EF*, which indicates that the polygon is asymmetrically distributed between the two sides of *MN*, the major axis of the MB box. The area of the polygon in the lower left quarter is much larger than the opposite.

Suppose the area and perimeter of a polygon are given by PA and PP, respectively; the area and perimeter of the MB box is MBA and MBP, respectively, the length and width of the MB box are L and W, respectively, and the orientation of the MB box and MWB box are θ_{MB} and θ_{MWB}, respectively.

Figure 2 is here.

If $\theta_{MB} = \theta_{MWB}$ (or $|\theta_{MB} - \theta_{MWB}| < \delta, \delta$ is a user-defined threshold), the patch is symmetrical either around the major or the minor axis of the MB box. If symmetrical around the minor axis of the MB box, the centroid of the polygon lies on the minor axis of the MWB box (Figure 3(a)); if symmetrical around the major axis of the MB box, the centroid of the polygon lies on the minor axis of the MWB box (Figure 3(b)). In either situation, the centroid passes through the major and minor axes of the MB box simultaneously.

Figure 3 is here.

Novel shape indices can then be derived (Table 1), including the MBLW (the length-to-width ratio of MB box), PAMBA (area ratio between patch and MB box), PPMBP (perimeter ratio between patch and MB box) and ODI (orientation difference index between MB and MWB boxes).

Table 1 is here.

3 Study area and data

The study area is located between 122°03′41’’E – 124°38′45’’E and 43°54′58″N – 45°45′50’’N, the hinterland of western Songnen Plain, Northeast China, covering the western Jilin Province and the Inner Mongolia Autonomous Region (Figure 4). The climate of this area is characterized as temperate continental monsoon ranging from semi-humid to semi-arid with an annual average temperature of 4 ℃ (Chi and Wang 2010). Annual mean precipitation is around 370-400 mm with 80% of the rainfall in July and August, causing a moisture deficit during 7 months of the year (Wang *et al.*

2009). However, the annual evaporation reaches 1700-1900 mm on average, about 4-5 times greater than precipitation. Such high levels of evaporation result in large areas of land degradation into saline soils throughout the study area.

Figure 4 is here.

The salt-affected soils are developed by several natural environmental factors, such as climate, geology, parent material, hydrological conditions, and freeze-thaw. There is evidence that a large paleolake in this area was formed after the Triassic Era by seawater incursion events due to tectonic activities (Huang *et al.* 2013). The paleolake gradually shrank in the Late Pleistocene due to the slow rise of the Songnen Plain and a long-term dry cold climate, and broke into hundreds of lake groups. These geological and geomorphological processes resulted in different degrees of salinity in different regions with distinctive geometric patterns. According to reference maps provided by local experts and soil scientists, the saline soils comprise of slightly saline, moderately saline, severely saline and “other” classes. The slightly saline soils along the large paleolake shore, are geographically located at the southern shore of the large paleolake with strongly oriented and elongated patterns; the moderately saline soils are distributed around current lakes with circular or half-moon shapes; the severely saline soils mostly lie in the central region of the large paleolake, which are large sized, irregularly distributed over the space with some connections between them (Qiu *et al.* 2012); the “other” saline soil type is uncertain in geometry, location and saline degree and, thereby, is ignored in this study.

Three cloud-free scenes acquired by the Landsat 8 OLI sensor on 15 September 2014 (Path 120, Row 28-29 and Path 119 Row 29) were used in this research. The images were composed of seven multispectral bands (Coastal Aerosol, Blue, Green, Red, NIR, SWIR1 and SWIR2) with a spatial resolution of 30 m. After radiometric and geometric correction, the images were segmented by a multi-resolution segmentation algorithm followed by spectral difference segmentation using the eCognition software to obtain vector or polygon data representing the saline soil patches with an overall classification accuracy of 90%. These saline soil vector polygons form the input data for the landscape pattern analysis and for validating the method. Note, because of the high spectral similarity, different saline soil type patches are unable to be discriminated based on spectra alone.

Ancillary data used in this paper, mainly as reference, include: 1) the National Land Cover Database (NLCD) of China to check the segmentation results, 2) Reference maps of different saline soil types provided by local experts for classification validation, 3) Obview-3 Panchromatic images and other fine spatial resolution imagery for visual interpretation, and 4) geophysical data (ASTER GDEM and Geomorphological Map) of the study area to understand the potential driving forces of landscape pattern. All these data were pre-processed and stored in ArcGIS coverage within the same coordinate system.

4 Results

4.1 Saline soil feature extraction based on rules involving novel shape indices

The feature extraction rules for each saline soil type were built on novel shape indices, in which the thresholds for each parameter were established using a mix of expert opinion (from saline soil scientists) coupled with a small amount of trial and error. The final rule sets for feature extraction for the three saline soil classes, namely the slightly saline soil, moderately saline soil and severely saline soil, are listed in Table 2, which will be elaborated as follows:

Table 2 is inserted here.

The slightly saline soil patches are located mainly in the southern shore of the large paleolake. They are characterized by strong patch symmetry around the major axis of the MB box and patch elongation with roughly east-west orientation, resulting in a very small threshold of ODI (<= 4.6) and a large threshold of MBLW (> 3); in addition, the slightly saline soil patches have a relatively larger PAMBA (> 0.34). Figure 5(a) illustrates a region of such saline soil patches, each of which has a narrow, long and almost coincident MWB box (in blue) and MB box (in red).

Surrounding current lakes, the moderately saline soil patches are usually characterized as having circular or half-moon shapes, that is, the patches are curved rather than elongated. Therefore, they have a low MWBLW (<2.8) and a low PAMBA value, within (0.18, 0.57); at the same time, they have a low PPMBP (< 2.22) in comparison with severely saline soil. Figure 5(b) demonstrates a region of such saline soil patches together with their MWB and MB boxes. From the figure, it can be seen that the PAMBA and the PPMBP of the patches are small, and the MBLW is also relatively small, with some MB boxes even close to square. Additionally, unlike the slightly saline soil patches, the MWB and MB boxes of some moderately saline soil patches are clearly not coincident (i.e. having relatively large ODI values).

Patches of severely saline soil are usually distributed at the centre of the large paleolake, commonly with contagion between them, with large shape size and a high shape complexity. The feature extraction rules for the severely saline soil patches were developed using a large threshold (>4,000.00 ha) of patch area and a large value of PPMBP (> 3.4). The resulting features, thus, have large areas with geometrically irregular shapes, as illustrated by Figure 5(c).

Figure 5 is inserted here.

Using the feature extraction rule sets (Table 2), the final classification of saline soil type (Figure 6) was produced, which includes four kinds of saline soils (i.e. slightly saline soil, moderately saline soil, severely saline soil and other saline soils). It should be noted that, the other saline soils were not identified with feature extraction rules; instead, they were identified as the residual patches not identified as one of the three former kinds. As the figure shows, the slightly saline soil consists of 45 patches (in green), distributed mainly in the south, coinciding with the southern shore of the large paleolake; the moderately saline soil class is composed of 127 patches (in blue), distributed mainly in the east, a place where current lakes are widespread and occupied by the interior of the large paleolake; the severely saline soil type includes five large and highly contagious patches (in reddish orange), located mainly in the north, coinciding with the centre of the large paleolake. The patch numbers, the mean patch size, total area, mean patch perimeter and total patch perimeter of each saline soil class were computed and are listed in Table 3. The saline soil classification accuracy was further assessed using stratified random sample points collected from reference maps provided by experts in paleogeography and soil science. The overall accuracy of the saline soil classification is up to 92.23% with a Kappa index of 0.84, which is a highly accurate classification result.

Figure 6 is inserted here.

Table 3 is inserted here.

4.2 Feature separability of novel and traditional shape indices

The transformed divergence (TD) separability and Jeffries-Matusita (JM) distance (italic) statistics for the novel indices, to be used in defining the rule sets for classifying the three saline soil classes, are summarized in Table 4. Here, the values in bold font indicate the high separability of a specific saline soil type from other classes based on the corresponding rule sets. In general, high separability (mostly greater than 1.8) was achieved by the proposed shape indices used to define the rule sets for each saline soil class. In terms of the slightly saline soil class, the three indices, namely ODI, MBLW and PAMBA, obtained a very high TD separability, larger than 1.9, even up to 2 (perfectly separable) when differentiating from the severely saline soil classes. Meanwhile, low TD and JM (1.4843, *1.3408*) between moderately saline soil and severely saline soil were realized for the three indices, but this has no impact on the feature extraction of the saline soil class in question (i.e. the slightly saline soil). With respect to the moderately saline soil class, the three novel indices (i.e. MBLW, PAMBA and PPMBP), also produced a very high TD separability (>1.9), and a high separability (around 1.8) is, surprisingly, produced between the two other saline soil classes (the slightly saline soil and the severely saline soil). As for the severely saline soil class, a perfect separability (around 2) was realized by patch area and PPMBP. But a very low TD and JM (1.3408, *0.8335*) between the slightly saline soil and the moderately saline soil occurred in this circumstance, revealing the inability of these two indices to distinguish the two saline soil classes.

Table 4 is inserted here.

As benchmarks, three traditional shape indices including the perimeter-area ratio (PARA) (Baker and Cai 1992, Hulshoff 1995, Garrabou *et al.* 1998, Saura and Carballal 2004), fractal dimension (*FRAC*) (Feder 1988, Leduc *et al.* 1994), and shape index (*SI*) (Saura and Carballal 2004) (see Table 5 for their detailed description) were tested for discriminating jointly between the three saline soil classes. The corresponding TD separability and JM (italic) values were computed and listed in Table 6. It can be seen from the Table 6 that, using the traditional indices, only the slightly and the severely saline soil classes are separable with high TD separability (>1.8), while the separability

(1.2962) between the slightly and the moderately saline soil classes and that (1.617) between the severely and the moderately saline soil classes are all relatively low.

Table 5 is inserted here.

Table 6 is inserted here.

5 Discussion

5.1 Minimum bounding rectangles

The minimum area bounding (MAB) box (i.e. the region bounding rectangle enclosing the minimum area) and its corresponding length-to-width ratio has been used to characterize the elongatedness of image objects, mainly for the purpose of remote sensing classification (Lewis *et al.* 1997, Jiao *et al.* 2012). However, when emphasising the minimum area of a rectangle, the patch directionality deriving from the ratio between the length and width of the rectangle is commonly ignored. The MB box, however, is built upon the moment orientation (MO), in which both the position and the area distribution of the patch (i.e. the inner structure of the patch) are taken into account (Zhang *et al.* 2006). Thus, it is a sensitive way to represent patch orientation. As shown by Figure 7, the directional deviation of the patch between the MAB box and the MB box is the greatest. As for the MWB box, due to the consideration of the minimum width of the rectangle, its length is highlighted, thereby enhancing its capability to represent patch directionality. As exemplified by Figure 7, the MWB box lies in the middle of the MAB box and the MB box, but closer to the MB box. From the mechanical point of view, the MB box is exactly constructed by two orthogonal principal stresses along the major axis and the minor axis, respectively (Timoshenko and Gere 1972). Such a mechanical characteristic is basically captured with the MWB box, except that the MWB box is invariant as long as the change of patch area and distribution remains within the current MWB box. Thus, while the MB box acts as a sensitive “detector” of patch geometry, the MWB box can serve as a benchmark. In fact, the formation of an anisotropic landscape can be regarded as the influence of natural and/or human forces, which can then be explained on the basis of mechanics. For anisotropic (i.e. vector) landscape analysis, therefore, the introduction and adoption of the MB and MWB boxes (both in possess of mechanical characteristics), instead of the MAB box, would be theoretically sound, despite the small (or even no) differences between them in some cases.

Figure 7 inserts here.

5.2 Novel shape indices

Four novel shape indices, namely patch length-to-width ratio (MBLW), area ratio between patch and MB box (PAMBA), perimeter ratio between patch and MB box (PPMBP) and orientation difference between MB and MWB boxes (ODI), were derived on the basis of the two different bounding boxes (i.e. MB and MWB boxes). Multiple aspects of patch-based landscape information including patch elongation, patch compactness, patch roughness and patch symmetry can, thus, be captured, which are especially needed for anisotropy-based landscape analysis. The effectiveness of the proposed indices were tested with real landscape data consisting of the three saline soil classes, namely slightly saline soil, moderately saline soil, and severely saline soil. These self-patterned patches of different saline soil classes are located in different geological and geographical environments (along the shore of the large paleolake, surrounding current lakes, lying in the centre of the large paleolake); they were developed under distinctive geophysical processes and formed with different landscape patterns including strip-like (elongated) shapes, circular or half-moon shapes, and large and irregular shapes (Qiu *et al.* 2012). The proposed indices were able to capture multiple aspects of patch-based landscape information relating to each saline soil class, with high TD separability values achieved for all pairs of saline soil classes (Table 4), even up to a very high separability between the slightly saline soil class and other classes. Traditional shape indices derived based on perimeter-area relationships (Saura and Carballal 2004), in contrast, attained low TD values for all pairs of saline soil classes except for the moderately saline soil and the severely saline soil (Table 6). These indices had difficulty in distinguishing some anisotropic and non-anisotropic patches, due to the existence of similar or even equal perimeter-area values among them.

5.3 General applicability of novel shape indices

The new boxes and indices proposed in this paper support quantitative modelling and analysis of anisotropic landscapes. Moreover, the formation of anisotropic landscapes is often associated with natural and/or anthropogenic driving forces. Each of the proposed indices captures a particular ecological characteristic, which can aid ecological interpretation and understanding. For example:

(i) the patch length-to-width ratio (MBLW) reflects the degree of anisotropy; the much larger MBLW value of the slightly saline soil patches reveals that this type of saline soil has a much higher anisotropy than the other two types;

(ii) the area ratio between a patch and its MB box (PAMBA) indicates whether an anisotropic patch is influenced by disturbance within the patch or along its boundary (like the moderately saline soil patches), which allows further analysis of the related driving forces;

(iii) the perimeter ratio between a patch and its MB box (PPMBP) reflects the roughness of an anisotropic patch, which is a measure of the natural degree of the patch boundary. It can also be used to quantify the contagiousness of a landscape patch, for instance, the high PPMBP value of the severely saline soil patches explains the obvious contagiousness of the patches.

With such multi-dimensional quantitative information, the pattern-process relationship of various anisotropic landscape patterns can be better understood, primarily in landscape ecology, but also in a wide range of other potential fields (e.g. sand dune development, forest fire spread, flood modelling, etc.).

5.4 Limitations of the novel indices

Novel indices were proposed for anisotropic, vector-based landscape analysis. For those patches whose length-to-width ratio is close to 1, application of these indices can lead to some uncertainties. Further, the new indices might be less sensitive to shape complexity for non-anisotropic landscape patterns than traditional shape indices. This is because the new indices are derived based on the oriented bounding rectangles, in which just one of the two patch parameters (patch area or patch perimeter) might be utilized. In traditional shape indices, however, both of the two parameters are incorporated simultaneously. This is why a high TD separability value for the moderately and severely saline soil classes was obtained by traditional indices (Table 6). No single measurement or index of shape can unambiguously differentiate all shapes (Forman 1995, Saura and Carballal 2004, Zhang *et al.* 2006). Combination of novel and traditional shape indices might be necessary for some complex landscape analysis. In fact, the identification of the severely saline soil patches combined both PPMBP and patch size.

5.5 Future research

The combination of minimum width bounding (MWB) box and moment bounding (MB) box, offers a flexible approach for patch structural analysis. ODI, for example, may be further divided into two categories: (1) ODI$<\delta$, the patch is symmetrical; and

(2) ODI $> \delta$, the patch is asymmetrical. For the case of ODI$< \delta$, two situations can be further divided: patch symmetry around the major axis of the MB box, and patch symmetry around the minor axis of the MB box. In fact, some patches of the moderately saline soil developed asymmetrically around the long sides of a patch (e.g. Figure 3(a)) often belonging to the latter; whereas most of the slightly saline soil patches belong to the former (e.g. Figure 3(b)). At the same time, a positive direction index can be assigned to the patch once the ratio between the distance of a patch centroid to the MWB box's centroid and half of the MWB box length surpasses a user defined threshold (e.g., the positive direction of the patch shown by Figure 3(b) is from left to right). For the case of ODI $> \delta$, two situations, namely left-handed rotation and right-handed rotation may further be deduced according to the relations between the two major axes. All these cases illustrate that patch heterogeneity can appear at the two ends of the major or minor axis, or around one of the axes. Moreover, new shape metrics for purely geometric representation might be deduced. For example, indices of "L-shape", "T-shape" "cross-shape (+)", etc. might be designed for building object-based remote sensing image segmentation. At the same time, as explained above, the proposed indices have great potential utility in a wide range of applications, including landscape ecology. Future research should be undertaken both to investigate the applicability and utility of the proposed techniques in these fields, as well as to develop them further.

6 Conclusion

Two minimal bounding rectangles (i.e. minimal width bounding (MWB) box and moment bounding (MB) box), suitable for anisotropic landscape analysis, were introduced in this research. Moreover, four new shape metrics, namely MBLW (the length-to-width ratio of MB box), PAMBA (area ratio between patch and MB box), PPMBP (perimeter ratio between patch and MB box) and ODI (orientation difference index between MB and MWB boxes), were introduced to quantify multiple aspects of landscape pattern including patch elongation, patch compactness, patch roughness and patch symmetry. These boxes and indices allow quantification of patch directionality and shape complexity simultaneously, which is especially suitable for anisotropic landscape pattern analysis. The experiment with real landscape data consisting of three saline soil classes demonstrated that the proposed indices measure multiple geometric dimensions of an anisotropic landscape, and led to a more accurate and robust classification of soil type than traditional shape indices.

7 Acknowledgements

This research was supported by the European Union Erasmus Mundus Scholarship [grant number 2011-0155] and co-funded by the Lancaster University Research Fund. The authors are grateful to Professor Shanwen Qiu at Northeast Institute of Geography and Agro-ecology, Chinese Academy of Sciences, for his expertise on saline soil rule set development. The authors would also like to thank the two anonymous referees for their constructive comments on this manuscript.

References

Baker, W.L. and Cai, Y., 1992. The r.le programs for multiscale analysis of landscape structure using the GRASS geographical information system. *Landscape Ecology*, 7 (4), 291–302.

Bolliger, J., Wagner, H.H., and Turner, M.G., 2007. *Identifying and Quantifying Landscape Patterns in Space and Time*. A Changing World. Springer Netherlands.

Chaudhuri, D. and Samal, A., 2007. A simple method for fitting of bounding rectangle to closed regions. *Pattern Recognition*, 40 (7), 1981–1989.

Chi, C.-M. and Wang, Z.-C., 2010. Characterizing Salt-Affected Soils of Songnen Plain Using Saturated Paste and 1:5 Soil-to-Water Extraction Methods. *Arid Land Research and Management*, 24 (1), 1–11.

Cissel, J.H., Swanson, F.J., and Weisberg, P.J., 1999. Landscape management using historical fire regimes: Blue River, Oregon. *Ecological Applications*, 9 (4), 1217–1231.

Corry, R.C. and Nassauer, J.I., 2005. Limitations of using landscape pattern indices to evaluate the ecological consequences of alternative plans and designs. *Landscape and Urban Planning*, 72 (4), 265–280.

Feder, J., 1988. *Fractals*. New York, NY, USA: Plenium Press.

Forman, R.T.T., 1995. Some general principles of landscape and regional ecology. *Landscape Ecology*, 10 (3), 133–142.

Forman, R.T.T. and Godron, M., 1986. *Landscape Ecology*. New York, NY, USA: John Wiley and Sons, Inc.

Fu, B. and Chen, L., 2000. Agricultural landscape spatial pattern analysis in the semi-arid hill area of the Loess Plateau, China. *Journal of Arid Environments*, 44 (3), 291–303.

Gardner, R.H. and O'Neill, R. V, 1991. *Pattern, process, and predictability: the use of neutral models for landscape analysis*. Quantitative methods in landscape ecology. New York, NY, USA: Springer-Verlag.

Garrabou, J., Riera, J., and Zabala, M., 1998. Landscape pattern indices applied to mediterranean subtidal rocky benthic communities. *Landscape Ecology*, 13 (4), 225–247.

Gertsev, V.I., 2004. Classification of mathematical models in ecology. *Ecological Modelling*, 178 (3-4), 329–334.

Grimm, V., Revilla, E., Berger, U., Jeltsch, F., Mooij, W.M., Railsback, S.F., Thulke, H.-H., Weiner, J., Wiegand, T., and DeAngelis, D.L., 2005. Pattern-oriented modeling of agent-based complex systems: lessons from ecology. *Science*, 310 (5750), 987–991.

Gustafson, E.J., 1998. Quantifying Landscape Spatial Pattern: What Is the State of the Art? *Ecosystems*, 1 (2), 143–156.

Gustafson, E.J. and Parker, G.R., 1992. Relationships between landcover proportion and indices of landscape spatial pattern. *Landscape Ecology*, 7 (2), 101–110.

Helfenstein, J., Bauer, L., Clalüna, A., Bolliger, J., and Kienast, F., 2014. Landscape ecology meets landscape science. *Landscape Ecology*, 29 (7), 1109–1113.

Van Den Hoek, J., Burnicki, A.C., Ozdogan, M., and Zhu, A.-X., 2015. Using a pattern metric-based analysis to examine the success of forest policy implementation in Southwest China. *Landscape Ecology*, 30 (6), 1111–1127.

Huang, Y., Yang, G., Gu, J., Wang, P., Huang, Q., Feng, Z., and Feng, L., 2013. Marine incursion events in the Late Cretaceous Songliao Basin: Constraints from sulfur geochemistry records. *Palaeogeography, Palaeoclimatology, Palaeoecology*, 385, 152–161.

Hulshoff, R.M., 1995. Landscape indices describing a Dutch landscape. *Landscape Ecology,* 10 (2), 101–111.

Jiao, L., Liu, Y., and Li, H., 2012. Characterizing land-use classes in remote sensing imagery by shape metrics. *ISPRS Journal of Photogrammetry and Remote Sensing*, 72, 46–55.

Kaplan, D.A., Paudel, R., Cohen, M.J., and Jawitz, J.W., 2012. Orientation matters: Patch anisotropy controls discharge competence and hydroperiod in a patterned peatland. *Geophysical Research Letters*, 39 (17), 1–7.

Krummel, J.R., Gardner, R.H., Sugihara, G., O'Neill, R. V., and Coleman, P.R., 1987. Landscape Patterns in a Disturbed Environment. *Oikos*, 48 (3), 321–324.

Kupfer, J.A., 2012. Landscape ecology and biogeography: Rethinking landscape metrics in a post-FRAGSTATS landscape. *Progress in Physical Geography*, 36 (3), 400–420.

Lausch, A., Blaschke, T., Haase, D., Herzog, F., Syrbe, R.-U., Tischendorf, L., and Walz, U., 2015. Understanding and quantifying landscape structure – A review on relevant process characteristics, data models and landscape metrics. *Ecological Modelling*, 295, 31–41.

Leduc, A., Prairie, Y.T., and Bergeron, Y., 1994. Fractal dimension estimates of a fragmented landscape: sources of variability. *Landscape Ecology*, 9 (4), 279–286.

Legendre, P. and Fortin, M.J., 1989. Spatial pattern and ecological analysis. *Vegetatio*, 80 (2), 107–138.

Lewis, H.G., Cote, S., and Tatnall, A.R.L., 1997. Determination of spatial and temporal characteristics as an aid to neural network cloud classification. *International Journal of Remote Sensing*, 18 (4), 899–915.

Li, B.L., 2000. Fractal geometry applications in description and analysis of patch patterns and patch dynamics. *Ecological Modelling*, 132 (1-2), 33–50.

Li, Y., Li, Y., Qureshi, S., Kappas, M., and Hubacek, K., 2015. On the relationship between landscape ecological patterns and water quality across gradient zones of rapid urbanization in coastal China. *Ecological Modelling*, 318, 100–108.

Markofsky, S. and Bevan, A., 2012. Directional analysis of surface artefact distributions: A case study from the Murghab Delta, Turkmenistan. *Journal of Archaeological Science,* 39 (2), 428–439.

McGarigal, K. and McComb, W.C., 1995. Relationships between landscape structure and breeding birds on the Oregon Coast Range. *Ecological Monographs*, 65 (3), 235–260.

McGarigal, K., Tagil, S., and Cushman, S.A., 2009. Surface metrics: An alternative to patch metrics for the quantification of landscape structure. *Landscape Ecology,* 24 (3), 433–450.

O'Neill, R. V., Krummel, J.R., Gardner, R.H., Sugihara, G., Jackson, B., DeAngelis, D.L., Milne, B.T., Turner, M.G., Zygmunt, B., Christensen, S.W., Dale, V.H., and Graham, R.L., 1988. Indices of landscape pattern. *Landscape Ecology*, 1 (3), 153–162.

Qiu, S., Wang, X., Zhang, S., Lian, Y., Zhang, Z., and Zhu, J., 2012. The evolution of the large paleolake in Songliao Plain and its formation. *Quaternary Sciences*, 32 (5), 1011 –1021 (in Chinese).

Reddy, C.S., Sreelekshmi, S., Jha, C.S., and Dadhwal, V.K., 2013. National assessment of forest fragmentation in India: Landscape indices as measures of the effects of fragmentation and forest cover change. *Ecological Engineering*, 60, 453–464.

Remmel, T.K. and Csillag, F., 2003. When are two landscape pattern indices significantly different? *Journal of Geographical Systems*, 5 (4), 331–351.

Remmel, T.K. and Fortin, M.J., 2013. Categorical, class-focused map patterns: Characterization and comparison. *Landscape Ecology*, 28 (8), 1587–1599.

Riitters, K.H., O'Neill, R. V., Hunsaker, C.T., Wickham, J.D., Yankee, D.H., Timmins, S.P., Jones, K.B., and Jackson, B.L., 1995. A factor analysis of landscape pattern and structure metrics. *Landscape Ecology*, 10 (1), 23–39.

Rossi, R.E., Mulla, D.J., Journel, A.G., and Franz, E.H., 1992. Geostatistical tools for modeling and interpreting ecological spatial dependence. *Ecological Monographs*, 62 (2), 277–314.

Saura, S. and Carballal, P., 2004. Discrimination of native and exotic forest patterns through shape irregularity indices: An analysis in the landscapes of Galicia, Spain. *Landscape Ecology*, 19 (6), 647–662.

Schröder, B. and Seppelt, R., 2006. Analysis of pattern-process interactions based on landscape models-Overview, general concepts, and methodological issues. *Ecological Modelling,* 199 (4), 505–516.

Seto, K.C. and Fragkias, M., 2005. Quantifying spatiotemporal patterns of urban land-use change in four cities of China with time series landscape metrics. *Landscape Ecology*, 20 (7), 871–888.

Stigler, S.M., 1981. Gauss and the Invention of Least Squares. *The Annals of Statistics*, 9 (3), 465–474.

Syrbe, R.U. and Walz, U., 2012. Spatial indicators for the assessment of ecosystem services: Providing, benefiting and connecting areas and landscape metrics. *Ecological Indicators*, 21, 80–88.

Timoshenko, S. and Gere, J.M., 1972. *Mechanics of Materials*. New York, NY, USA: Van Nostrand Reinhold Co.

Tischendorf, L., 2001. Can landscape indices predict ecological processes consistently? *Landscape Ecology*, 16 (3), 235–254.

Toussaint, G., 1983. Solving geometric problems with the rotating calipers. *In*: *IEEE MELECON83*. 1–8.

Turner, M.G., 1990. Spatial and temporal analysis of landscape patterns. *Landscape Ecology*, 4 (1), 21–30.

Turner, M.G., 2005. Landscape Ecology: What Is the State of the Science? *Annual Review of Ecology, Evolution, and Systematics*, 36, 319–344.

Uuemaa, E., Mander, Ü., and Marja, R., 2013. Trends in the use of landscape spatial metrics as landscape indicators: A review. *Ecological Indicators*, 28, 100–106.

Vidal Vázquez, E., Vivas Miranda, J.G., and Paz González, A., 2005. Characterizing anisotropy and heterogeneity of soil surface microtopography using fractal models. *Ecological Modelling*, 182 (3-4), 337–353.

Vogt, P., Riitters, K.H., Estreguil, C., Kozak, J., Wade, T.G., and Wickham, J.D., 2007. Mapping spatial patterns with morphological image processing. *Landscape Ecology*, 22 (2), 171–177.

Wang, L., Seki, K., Miyazaki, T., and Ishihama, Y., 2009. The causes of soil alkalinization in the Songnen Plain of Northeast China. *Paddy and Water Environment*, 7 (3), 259–270.

Wu, J., 2013. Key concepts and research topics in landscape ecology revisited: 30 years after the Allerton Park workshop. *Landscape Ecology*, 28 (1), 1–11.

Wu, J., Jelinski, D.E., Luck, M., and Tueller, P.T., 2000. Multiscale Analysis of Landscape Heterogeneity: Scale Variance and Pattern Metrics. *Annals of GIS*, 6 (1), 6–19.

Yuan, J., Cohen, M.J., Kaplan, D.A., Acharya, S., Larsen, L.G., and Nungesser, M.K., 2015. Linking metrics of landscape pattern to hydrological process in a lotic wetland. *Landscape Ecology*, 30 (10), 1893–1912.

Zaslavsky, D. and Rogowski, A.S., 1969. Hydrologic and Morphologic Implications of Anisotropy and Infiltration in Soil Profile Development. *Soil Science Society of America*

Journal, 33 (4), 594–599.

Zhang, S., Zhang, J., Li, F., and Cropp, R., 2006. Vector analysis theory on landscape pattern (VATLP). *Ecological Modelling*, 193 (3-4), 492–502.

Tables

Table 1 Detailed description of novel shape metrics.

Indices (Acronym)	Formula	Description
patch length-to-width ratio (MBLW)	L/W	Description of **vector patch elongatedness** According to the ratio between length (m) and width (m) of MB: The MBLW ≧ 1. The lager the value, the more elongated the shape.
Area ratio between patch and MB box (PAMBA)	PA/MBA	Description of **vector patch compactness** According to the ratio between patch area (ha) and MB area (ha): The larger the value, the larger the filling degree and the more compact the shape.
Perimeter ratio between patch and MB box (PPMBP)	PP/MBP	Description of **vector patch roughness** According to the ratio between patch perimeter (m) and MB perimeter (m): The larger the value, the rougher the patch's edge.
Orientation difference (0-180) between MB and MWB (ODI)	$\lvert \theta_{MB} - \theta_{MWB} \rvert$	Description of **vector patch symmetry** If ODI < δ (δ is user defined threshold), the patch is symmetric; the smaller (the larger respectively) the value, the more symmetrical (asymmetrical respectively) the shape.

Table 2 Rule sets based on novel shape indices for saline soil feature extraction.

Class	Shape indices	Rules
slightly saline soil	ODI	<= 4.6
	MBLW	> 3
	PAMBA	> 0.34
moderately saline soil	MBLW	< 2.8
	PAMBA	(0.18 - 0.57)
	PPMBP	< 2.22
severely saline soil	Patch area	>= 4,000.00 (ha)
	PPMBP	> 3.4

Note: Intersection set operations within rule sets

Table 3 Area and number of patches of each saline soil class.

Saline soil class	Patch numbers	Mean patch area (ha)	total area (ha)	Mean patch perimeter (m)	Total perimeter (m)
slightly saline soil	45	3,417.18	153,773.10	83,983.36	3,779,251.35
moderately saline soil	127	521.67	66,251.92	20,805.78	2,642,333.99
severely saline soil	5	26,026.68	130,133.42	664,982.95	3,324,914.95

Table 4 Feature separability of novel shape indices corresponding to the rule sets.

Shape indices	Saline soil class	slightly saline soil	Moderately saline soil	Severely saline soil
ODI, MBLW and PAMBA	Slightly saline soil	—	*1.7593*	***1.9857***
	Moderately saline soil	**1.9361**	—	*1. 3408*
	Severely saline soil	**2.0000**	1.4843	—
MBLW, PAMBA and PPMBP	Slightly saline soil	—	***1.9316***	*1.7562*
	Moderately saline soil	**1.9685**	—	***1. 9408***
	Severely saline soil	1.8741	**1.9843**	—
Patch area and PPMBP	Slightly saline soil	—	*0.8335*	***1.9441***
	Moderately saline soil	1.3408	—	***1.9343***
	Severely saline soil	**1.9961**	**2.0000**	—

Table 5 Detailed description of traditional shape metrics.

Shape index	Formula	Description
Mean perimeter-area ratio (*MPAR*)	$MPAR = \frac{p}{a}$	The ratio between patch perimeter (*m*) and area (*ha*)
fractal dimension (*FD*)	$FD = \frac{2\ln(p) - \ln(k)}{\ln a}$	Here *k*=1.
Shape index (*SI*)	$SI = \frac{p}{2\sqrt{\pi}\sqrt{a}}$	*SI* attains its minimum (*SI* = 1) for circles and increases (with no upper limit) for more complex or elongated shapes

Note: *p* and *a* are, respectively, the perimeter and area of the patch

Table 6 The TD separability and JM distance (italic) of the three traditional shape indices.

Saline soil class	Slightly saline soil	Moderately saline soil	Severely saline soil
Slightly saline soil	—	*1.1129*	*1.7397*
Moderately saline soil	1.2962	—	*1.4886*
Severely saline soil	1.8212	1.617	—

Figure captions

Figure 1. A patch (S) with centroid C ($\bar{x},\bar{y}$), *dA* is the differential area of point (*x*, *y*), *oxy* is the geographic coordinate system.

Figure 2. A polygon with its MWB box (in blue) and MB (in red) box.

Figure 3. A polygon with its MWB box and MB box completely coincident. C is the centroid of the polygon, and AB and EF are the major and minor axes of the MWB box, respectively, and MN and PQ are the major and minor axes of the MB box, respectively. (a) the centroid lying on the minor axis of MWB; (b) the centroid lying on the major axis of MWB.

Figure 4. The Geographic location of study area.

Figure 5. Part of study area showing (a) slightly saline soil patches with their MWB and MB boxes, (b) moderately saline soil patches with their MWB and MB boxes and (c) severely saline soil patches with their MWB and MB boxes.

Figure 6. Different saline soil classes identified by the rule sets developed by the proposed novel indices.

Figure 7. A patch example with MB box (in red), MWB box (in blue) and MAB box (in green).

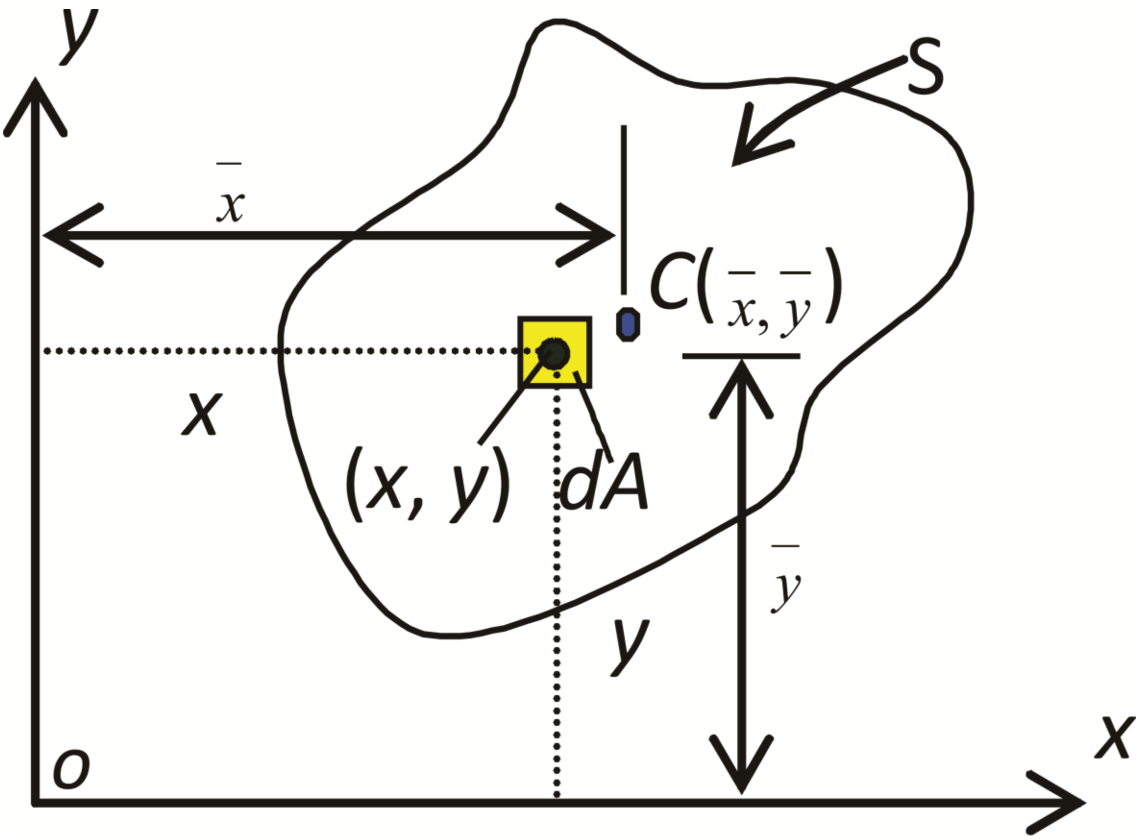
y
S
$\bar{x}$
C($\bar{x}$, $\bar{y}$)
x
(x, y)
dA
$\bar{y}$
y
x
o

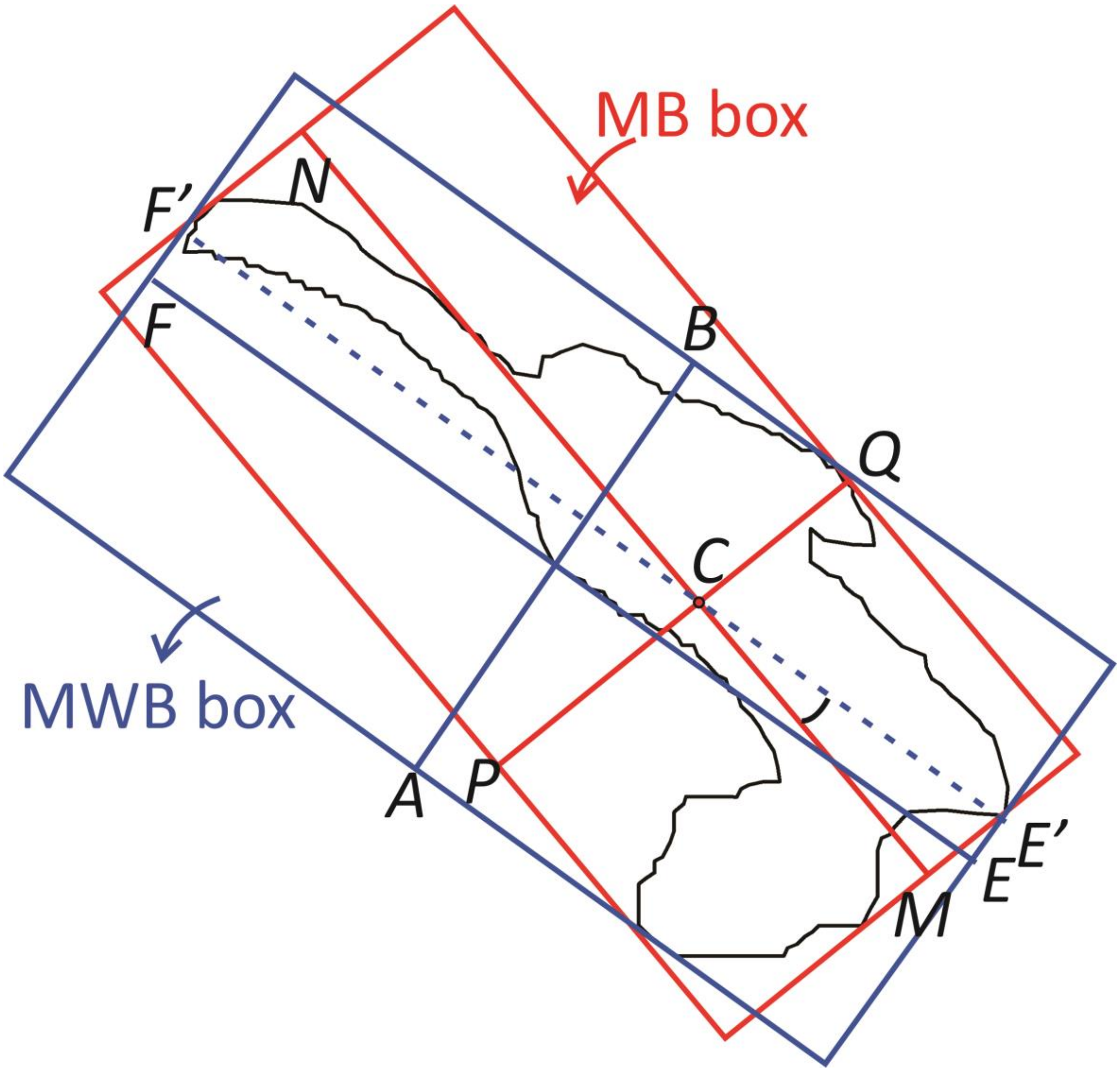
MB box
MWB box
F’
N
F
B
Q
C
A
P
M
E
E’

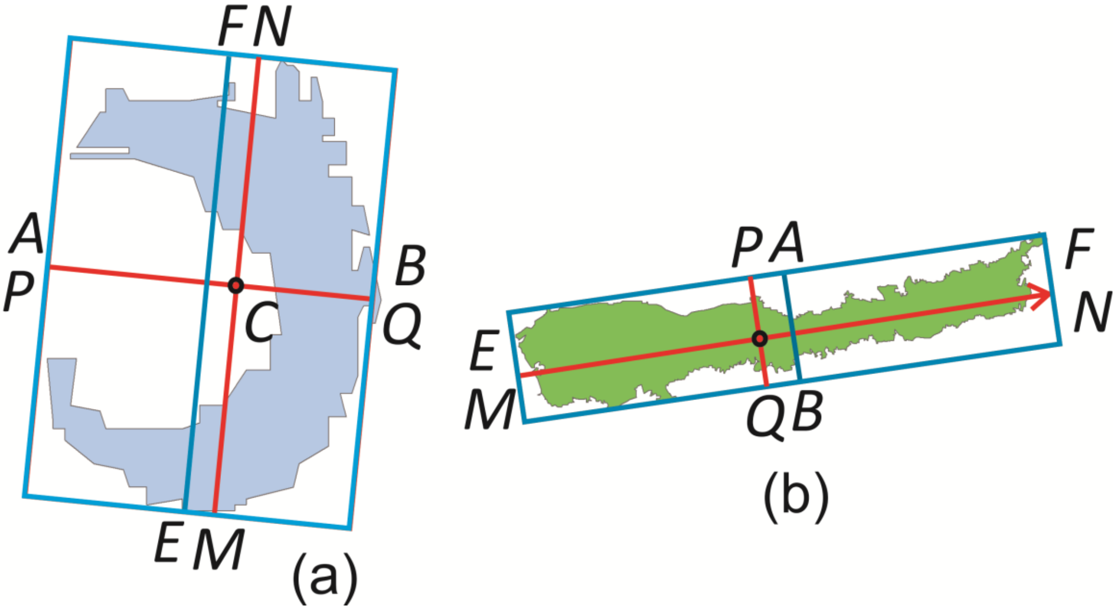
F N
A
P
B
C
Q
E M
(a)
P A
F
E
N
M
Q B
(b)

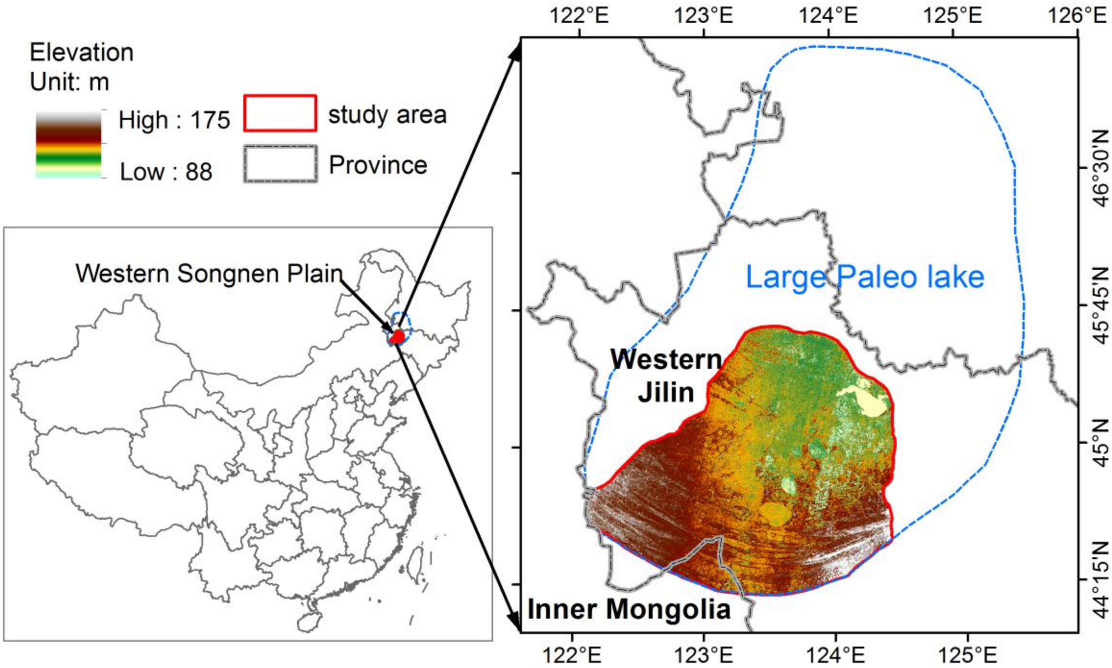
Elevation
Unit: m
High : 175
Low : 88
study area
Province
Western Songnen Plain
Large Paleo lake
Western Jilin
Inner Mongolia
122°E
123°E
124°E
125°E
126°E
46°30'N
45°45'N
45°N
44°15'N

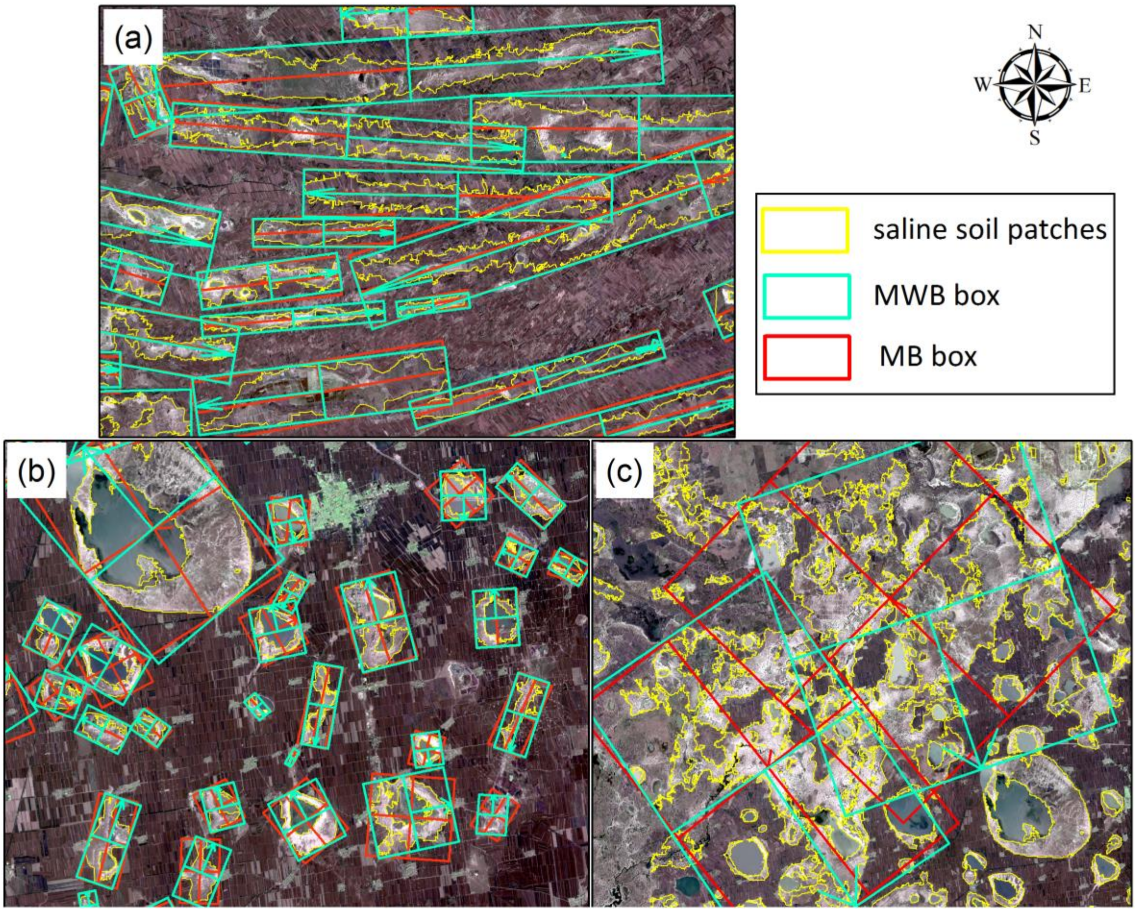
(a)
(b)
(c)
N
W
E
S
saline soil patches
MWB box
MB box

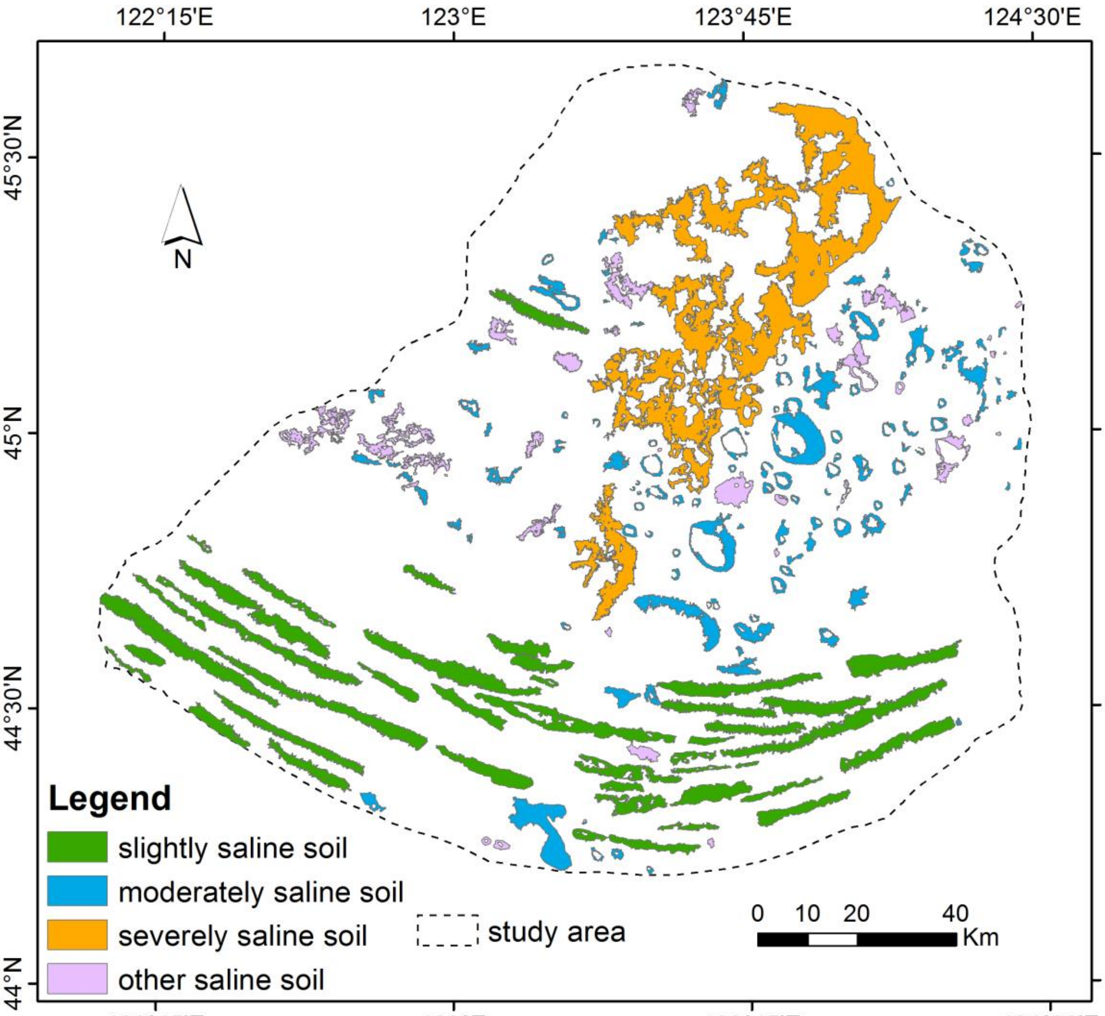
122°15'E
123°E
123°45'E
124°30'E
45°30'N
45°N
44°30'N
44°N
N
Legend
slightly saline soil
moderately saline soil
severely saline soil
other saline soil
study area
0 10 20 40
Km

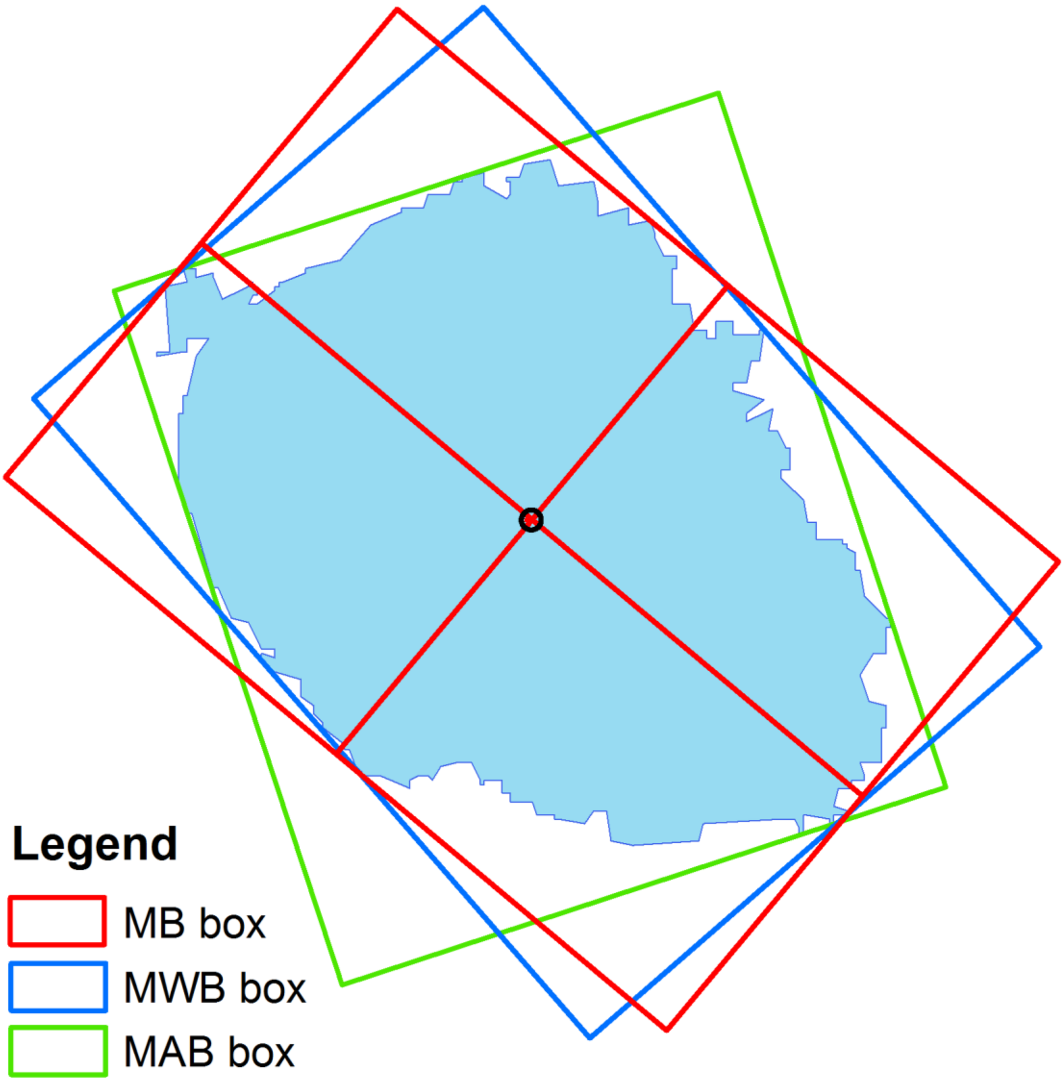

687